Appl. Phys. B (2017) 123:193
DOI 10.1007/s00340-017-6770-3

Applied Physics B
Lasers and Optics

Acetone photophysics at 282 nm excitation at elevated pressure and temperature. II: Fluorescence modeling

Jason Hartwig[1] · **Mandhapati Raju**[2] · **Chih-Jen Sung**[3]

Received: 17 February 2017 / Accepted: 6 June 2017 / Published online: 14 June 2017

Abstract This is the second in a series of two papers that presents an updated fluorescence model and compares with the new experimental data reported in the first paper, as well as the available literature data, to extend the range of acetone photophysics to elevated pressure and temperature conditions. This work elucidates the complete acetone photophysical model in terms of each and every competing radiative and non-radiative rate. The acetone fluorescence model is then thoroughly examined and optimized based on disparity with recently conducted elevated pressure and temperature photophysical calibration experiments. The current work offers insight into the competition between non-radiative and vibrational energy decay rates at elevated temperature and pressure and proposes a global optimization of model parameters from the photophysical model developed by Thurber (Acetone Laser-Induced Fluorescence for Temperature and Multiparameter Imaging in Gaseous Flows. PhD thesis, Stanford University Mechanical Engineering Department, 1999). The collisional constants of proportionality, which govern vibrational relaxation, are shown to be temperature dependent at elevated pressures. A new oxygen quenching rate is proposed which takes into account collisions with oxygen as well as the oxygen-assisted intersystem crossing component. Additionally, global trends in ketone photophysics are presented and discussed.

✉ Jason Hartwig
Jwh13@case.edu

[1] Department of Mechanical and Aerospace Engineering, Case Western Reserve University, Cleveland, OH 44106, USA

[2] Convergent Science Inc., Madison, WI 53719, USA

[3] Department of Mechanical Engineering, University of Connecticut, Storrs, CT 06269, USA

1 Introduction

Fluorescence is a radiative process between states of similar multiplicity that involves spontaneous emission of light. The highest probability de-excitation paths are non-radiative ones. For ketones such as acetone, crossover to the first excited triplet (T_1) occurs at near unity probability in many molecules due to closely spaced energy levels between the first excited singlet (S_1) and triplet states [2]. Emission energies are always smaller than absorption energies since one or more energy dissociative processes precede emission.

For laser-induced fluorescence (LIF), laser light tuned to a specific wavelength targets an absorbing species of interest in S_0. The light excites a fraction of the ground state molecules to an excited electronic state. The allowed transitions that form the absorption spectrum of the molecule are governed by spin and symmetry selection rules. Then, the fluorescent photons are converted to a working signal or image through the use of a detection system with appropriate filtering and collection optics. For a steady-state system, the signals are usually gated and integrated in time and processed to acquire a physical property of interest. Though somewhat complicated to model due to the existence of multiple relaxation paths, interpretation can be still straightforward and signal levels are typically high, because fluorescence involves electronic energy differences.

Thurber [1] introduced a basic model to describe acetone fluorescence and experimentally determined the fundamental dependence of fluorescence on excitation wavelength at varying temperature under 1 atm, as well as at varying pressure under constant temperature of 300 K. Although the fluorescence model of [1] was able to represent important photophysical features, there was considerable disparity between model and experimental data, even at the room

temperature, intermediate pressure and room pressure, high temperature range over which the model was validated. When extended to the coupled elevated pressure and temperature data, the model of [1] does not agree at all with the four available literature studies [3–6] or the current work [7]. Extension of the model of Thurber [1] to more practical engine-like environments, thus, requires further insight.

This is the second of two papers that presents updated fluorescence modeling to extend the range of acetone photophysics to elevated pressure and temperature conditions at an excitation wavelength near the absorption peak. The first of the two papers presented the experimental design, methodology, design validation, and experimental results for the system used to study both the independent and coupled effect of elevated pressure and temperature on acetone photophysics over pressures of 0.05–4.0 MPa and temperature of 295–750 K for 282 nm excitation wavelength in nitrogen (N_2) and air as bath gases. The purpose of this paper is to present the complete acetone photophysical and fluorescence models and model re-optimization based on new elevated pressure and temperature calibration data to enable acetone LIF to be applied as a diagnostic technique in high pressure and temperature systems. Specifically, for the purpose of advancing overall ketone fluorescence modeling, it is desired to validate/update the non-radiative rate, k_{nr}, as well as collisional constants, at higher excitation energies.

2 Background

2.1 General fluorescence

Information regarding general fluorescence may be summarized via a fluorescence rate, lifetime, or overall "quantum yield". Typically in LIF systems, one can measure the time dependence of the fluorescence,

$$\tau_f = \frac{1}{k_f + k_{coll} + k_{ic} + k_{isc} + k_{pd} + k_{td} + k_{o_2}}, \quad (1)$$

and/or the total fluorescence quantum yield (FQY):

$$\phi_f = k_f \tau_f = \frac{k_f}{\sum k_i}, \quad (2)$$

where the fluorescence k_f, collisional k_{coll}, internal conversion (IC) k_{ic}, intersystem crossing (ISC) k_{isc}, photodissociative k_{pd}, thermal dissociative k_{td}, and oxygen quenching rate k_{o_2} are represented, respectively [8]. Typically, the photodissociative rate is taken as a function of laser energy, and the thermal dissociative rate is a strong function of temperature. Although non-radiative rates cannot be measured directly, it is possible to infer the total non-radiative rate, assuming that these two physical observables, fluorescence lifetime and fluorescence quantum yield, have been obtained. Meanwhile, the oxygen quenching rate is taken as the oxygen quenching efficiency (the probability that a collision with an oxygen molecule will cause direct quenching to T_1), $\langle p \rangle$, times the product of oxygen number density, η_o, and oxygen collisional frequency Z_o [9]:

$$k_{o_2} = \langle p \rangle \eta_o Z_o. \quad (3)$$

2.2 Ketone photophysical model

Historically, ketones have been attractive fluorescing species for use in tracer LIF studies due to the fact that ketone LIF is dominated by fast ISC, reducing fluorescence signal complexity [10]. These polyatomic organic molecules exhibit a broadband absorption feature because of a high density of vibrational states in S_1. Ketone fluorescence from the S_1 follows absorption of ultraviolet (UV) laser light from the vibrationally allowed, symmetry forbidden $n \rightarrow \pi^*$ transition from the C–O bond, corresponding to the promotion of a nonbonding electron to an antibonding orbital. Compared to the $\pi \rightarrow \pi^*$ transition (promotion of a bonding electron to an antibonding orbital) associated with aromatics and alkenes, absorption strength and de-excitation energy transitions are generally weaker for ketones due to the inefficient transition of near orthogonal orbitals.

Fast vibrational relaxation in S_1 increases overall fluorescence signal levels and guarantees long emission wavelengths in the visible region [11]. The small fraction of excited state ketone molecules that have not undergone ISC to T_1 will quickly de-excite via collisions, and then fluoresce. Therefore, in ketones, the probability of fluorescence from lower vibrational levels is high. Since ISC involves a spin change, de-excitation from T_1 to S_0 occurs on a much longer time scale. Ketone phosphorescence is significantly quenched in the presence of even a small amount of oxygen because the ground state configuration of molecular oxygen is T_1. Thus, oxygen assists energy transfer and electron pairing in T_1.

2.3 Acetone photophysical model

2.3.1 Absorption

Typical ketone photophysical behavior is illustrated in Fig. 1 through the use of a Jablonski diagram, using acetone as the representative tracer. Acetone absorbs UV light in the wavelength range of 225–320 nm, peaking at 275 nm, and fluoresces in the visible range of 350–550 nm. The acetone absorption spectrum is broad and generally featureless. Vibrational structure has been resolved at lower acetone partial pressures [12]. Subsequently, Zuckermann and Haas [13] performed higher resolution studies of rotational structure in lower lying S_1 vibrational bands,

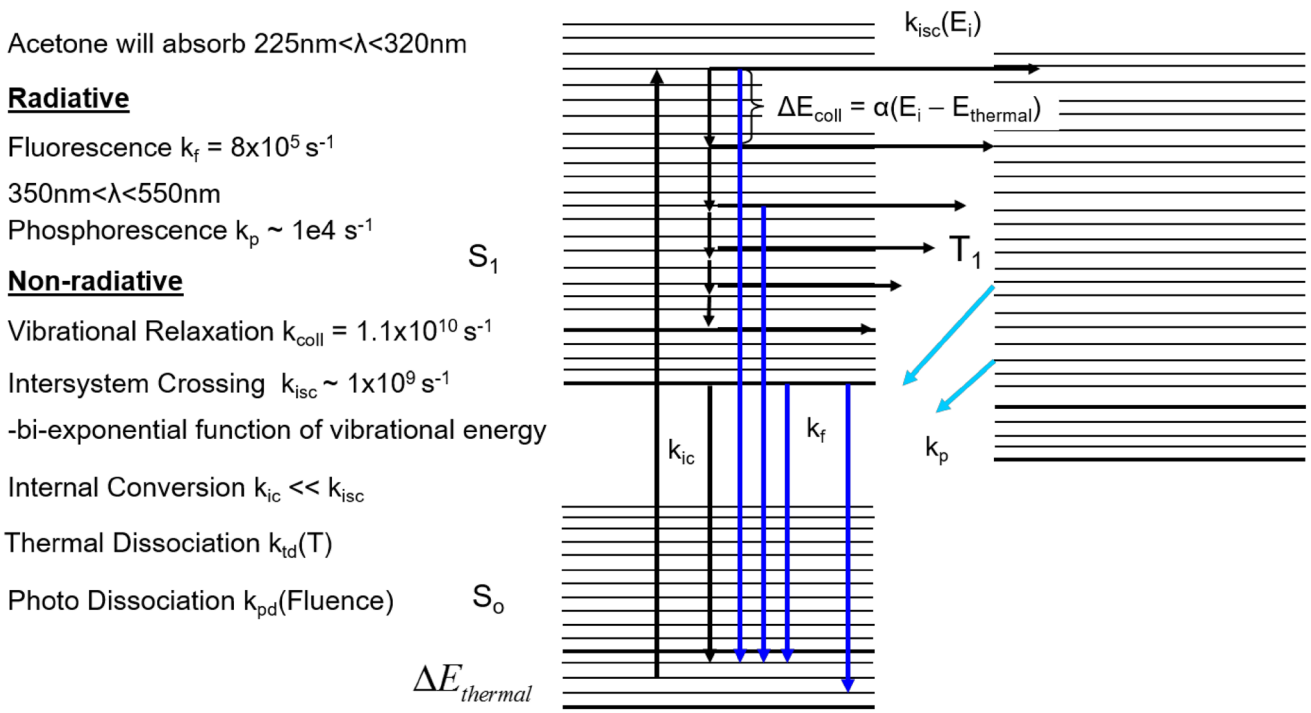

Fig. 1 Jablonski diagram for acetone vapor

detailing a constant threefold splitting of each line due to methyl group torsional motion. Vibrational frequencies and bond lengths and angles of S_1 were experimentally obtained and compared with calculations [14].

2.3.2 *Collisional rate*

Following acetone absorption to S_1, the most probable path for de-excitation involves either tracer–tracer or tracer–bath gas collision. As governed by the Stern–Volmer relationship, this gain in electronic energy is quickly transferred to and from the vibrational modes of the absorbing species via collision and is governed by a species-specific collisional rate, k_{coll}. Collisional de-excitation is favorable because the ratio of high energy ground state molecules to low energy excited state molecules is small.

Specific information about collisional energy transfer is indirectly obtained through the pressure dependence of fluorescence. The collisional rate itself is dependent on preponderant parameters such as temperature, pressure, and specific colliding partner and is derived through the Lennard-Jones equation. At standard temperature and pressure, the collisional rate for acetone in nitrogen bath gas is 1.07×10^{10} s^{-1}. All collisional parameters and Lennard-Jones calculations in this work were taken from [15].

Early on, the pressure dependence on fluorescence of large polyatomic molecules was studied [16, 17]; collisional probabilities showed strong dependence on excited state vibrational energy level and the specific colliding partner [18–22], such that the average energy transferred per collision can be defined in the following way:

$$\Delta E_{\text{coll}} = \alpha(E_i - E_{\text{thermal}}), \tag{4}$$

where E_i is the ith energy level above the thermalized level, E_{thermal} is the room temperature Boltzmann distribution, and α is the constant of proportionality loosely defined as a measure of the collision efficiency for a given bath gas. α is generally taken to be constant, and this linearity has been demonstrated through a relatively wide range of vibrational energies for large polyatomics such as toluene [20] and azulene [21]. However, there is deviation from linearity at both low and high pressures; collisional energy approaches zero for weak excitation and levels off for high excitation [23].

It was also verified through both experiment and computation that the amount of energy transferred per collision was approximately proportional to the number of atoms in the colliding partner for many large polyatomic molecules, including sec-butyl radicals [24], toluene [20], and azulene [23, 25]. Meanwhile, computational work also supported experimental evidence for stepwise collisional de-excitation [22, 26]. Normalized collisional information about a particular bath gas is obtained through the so-called reference collisional frequency and is available in the literature for many bath gases, see [20, 21, 25] for example. Although direct work on acetone collisional energy transfer is sparse,

the results of azulene and toluene are widely accepted and easily extended to other large polyatomics like acetone.

2.3.3 Intersystem crossing

As an acetone molecule de-excites through collisional events, it may undergo either a radiative or non-radiative process at any step. The second most probable path of de-excitation is a crossover to T_1. The ISC is defined as the non-radiative transition between two states of different spin quantum number. It is a highly probable event since energy levels of S_1 and T_1 are so closely matched (near coincidence) and transitions to the triplet state require significantly less energy than spontaneous fluorescence emission. Since ISC is a non-radiative phenomenon, one must infer its values and dependencies through experiments that reduce collisional effects by placing the excited state molecule closer to the thermalized level [27, 28]. By varying temperature or excitation wavelength, one can monitor changes in phosphorescence and, thus, deduce ISC rates.

For acetone and other large polyatomics, this ISC rate increases with increased vibrational energy in S_1 [10, 29, 30]. Early work in formulating the acetone mechanism showed an overall decrease in fluorescence with increased temperature [31]. Fluorescence lifetimes were approximated as the inverse of the non-radiative rates [10, 32]. The energy dependence of the non-radiative rate of acetone was further supported through examination of phosphorescence. Experimentalists varied excitation energy to study phosphorescence emission of "hot" triplets (i.e., higher lying state) as well as "thermalized" (lower lying states) triplets to further validate the energy dependence of k_{nr}, e.g., [17, 33]. For an excited state acetone molecule with average vibrational energy, the non-radiative rate is 2–3 orders of magnitude larger than the radiative rate.

2.3.4 Quenching due to oxygen

In the presence of oxygen, the ISC rate is further enhanced because of oxygen's natural triplet ground state. In previous works such as [31, 34], even minute amounts of oxygen were capable of completely quenching acetone phosphorescence. But the effect on acetone fluorescence was poorly understood until the studies of [4, 35]. Nau and Scaiano [36] determined a weak interaction between oxygen and ketone and diketone fluorescence and hypothesized an oxygen-enhanced ISC rate that was proportional to oxygen number density, which proceeds through an intermediate encounter complex that includes charge–transfer interactions [37]. At low enough oxygen partial pressures in Eq. 3, the rate resembles a collision frequency [38]; at high oxygen partial pressures, the rate will increase the overall ISC rate and quench acetone fluorescence.

2.3.5 Fluorescence and phosphorescence

The third most probable path of de-excitation is fluorescence or phosphorescence defined as direct, spontaneous emission of a photon from S_1 or T_1, respectively. Early work focused on low pressure applications to characterize acetone and biacetyl fluorescence yields on an absolute basis [32, 34, 39]. As indicated in these works, however, there was significant uncertainty and disparity among these early absolute fluorescence measurements. Information regarding acetone fluorescence and phosphorescence has been deduced through study of its decay rates [31, 33], its spectrum [10], and its pressure [35, 40], temperature [4, 41], and excitation wavelength [39, 41, 42] dependencies. Fluorescence (and phosphorescence) rates were assumed to be constant with vibrational level, as are most carbonyl compounds [8] so changes in the FQY are tracked through changes in the fluorescence lifetime.

Acetone phosphorescence rates ($k_p = 1 \times 10^4\ s^{-1}$) are slightly slower than fluorescence rates ($k_f = 1 \times 10^6\ s^{-1}$) because an electron occupying an excited T_1 state must first undergo spin change before photon emission and de-excitation back to S_0. Phosphorescence emission is red shifted and weaker in signal strength with respect to fluorescence since T_1 energy levels are, on average, slightly lower than their S_1 counterparts [33]. Since fluorescence can be spectrally separated from phosphorescence and since the two events occur at differing time scales, it is assumed that the minute amount of phosphorescence emission during fluorescence signal measurements is negligible.

2.3.6 Internal conversion

There are three other primary non-radiative de-excitation processes which are considered, including internal conversion, thermal dissociation, and photo destruction, all of which contribute to the acetone fluorescence mechanism. Internal conversion (IC) is defined as the de-excitation and rearrangement of a systems internal energy via collisions from the excited state thermalized level to the ground state. Molecules that have not emitted a photon after successive collisions in the excited state reach the thermalized level and eventually collide back to the ground state. Prior to experiments on IC, experimentalists assumed that the probability for IC was higher than that of ISC because IC only occurs between states with the same multiplicity [43]. However, it was experimentally and theoretically verified that most fluorescing species used in combustion studies have significantly low IC rates. For acetone, the probability for IC is

significantly less than that of fluorescence [11, 22, 44] and is thus ignored in all subsequent work presented here. In addition, the chemical and photo dissociation of acetone is neglected in this study, because the temperatures and pumping energies investigated were not extremely high.

3 Baseline acetone fluorescence modeling

In the past, thorough interpretation of acetone fluorescence was crippled by unknown collisional and/or quenching rates, especially quenching by oxygen. Also reducing model complexity was the fact that ketone ISC probabilities were near unity. Because of discrepancies in quantitative acetone fluorescence data, a new and comprehensive model was needed. First formulated by [1] and influenced heavily by [41], the model was central to progressing tracer LIF. At present time, it may only be treated as a semi-quantitative representation of the acetone fluorescence mechanism. Key parameters of the model may not yet be extracted as physical observables on a fundamental basis until fluorescence is characterized over the complete range of pressure, temperature, excitation wavelength, and bath gas. The fluorescence model is briefly described in this section; a more detailed discussion is reserved for the literature [1].

3.1 Model formulation

3.1.1 Assumptions

First, transitions of a single "average" molecule were considered so that second-order distortion effects on the ground state energy distribution introduced by the absorption cross section can be neglected, and the entire ensemble of molecules may be approximated by a single molecule [1]. Second, k_{ic}, k_{td}, and k_{pd} are ignored in the model; the physical and chemical dissociative effects introduced by high temperature and pumping energy were assumed to be negligible and only faults of experimental design. Third, the model simplifies the collisional rate by neglecting upward collisions and assumes a gradual downward collisional cascade in discrete energy steps of ΔE_{coll}, as theorized by [18, 26]. Fourth, k_{nr} is assumed irreversible. Fifth, perfect harmonic oscillators were assumed for the vibrational energy levels to allow for straightforward calculation of the average thermal energy at each iteration of the fluorescence calculation. Lastly, the model was fit to low pressure and temperature data from [1].

3.1.2 Overview

Table 1 lists original model parameters. Note that the pressure and temperature sensitive collisional rate and the energy-dependent non-radiative rate are evaluated at standard temperature and pressure; in the fluorescence model, they are calculated at each iteration. Model input parameters are excitation wavelength, partial pressure or mole fraction of the fluorescing species, and total gas temperature and pressure. Initially, an "average" molecule sits in thermal equilibrium in the ground state with an average energy determined solely by the Boltzmann distribution, $\Delta E_{thermal}$. Laser light tuned to a specific wavelength excites the molecule with photon energy equal to E_{laser}. Thus, the

Table 1 Baseline fluorescence model parameters

Model parameter	Value				
Radiative/non-radiative					
k_f [1/s][a]	8.0×10^5				
k_{nr} [1/s][b]	$-3.82 \times 10^9 + 8.82 \times 10^5 * \exp(E_i/1650) + 4.08 \times 10^9 * \exp(E_i/7.73 \times 10^4)$				
Model parameter	Value				
Collisional	N_2	He	CH_4	O_2	Air
k_{coll} [1/s][c]	1.067×10^{10}	1.304×10^{10}	1.444×10^{10}	9.988×10^9	1.051×10^{10}
α[d]	0.22	0.0098	0.03	0.22	0.22
Model parameter					Value
Quenching					
${}_{o2}k$[d]					$0.00399 * k_{coll,o_2}$

[a] Hansen and Lee [10]

[b] Breuer and Lee [27], Shortridge et al. [28], and Ossler and Alden [35]

[c] Value taken from [15], evaluated at 295 K, 1 atm

[d] Thurber [1]

initial vibrational energy, E_{initial}, of this "average" molecule in S_1 is approximated by

$$E_{\text{initial}} = \Delta E_{\text{thermal}} + E_{\text{laser}} - E_{\text{o}}, \tag{5}$$

where E_{o} is the energy difference between the lowest vibrational level of S_0 and S_1. For each vibrational level in S_1, the molecule can decay in discrete energy steps determined by the quantity $k_{\text{coll}}\Delta E_{\text{coll}}$, where ΔE_{coll} is defined in Eq. 4 and collisional properties may be calculated from Lennard-Jones parameters derived through knowledge of the bath gas. As the molecule decays, it may cross over to T_1 with a rate of $k_{\text{nr}}(E_i) = k_{\text{isc}}(E_i)$, quench directly in the presence of oxygen with a rate of k_{O_2}, spontaneously fluoresce to S_0 with a rate of k_{f}, or further decay through collision with a rate of $k_{\text{coll}}(T, P, \chi_{\text{bathgas}})$, where χ_{bathgas} is the mole fraction of the bath gas, en route to the thermalized level in S_1. Since IC is not considered, the molecule must then fluoresce or cross to T_1.

For a given pressure, temperature, and excitation wavelength, the total FQY may be calculated by summing the individual fluorescence contributions from each ith vibrational energy level through the following relationship:

$$\begin{aligned}\phi = &\frac{k_{\text{f}}}{k_{\text{f}} + k_{\text{coll}} + k_{\text{nr},1} + k_{O_2}} \\ &+ \left(\sum_{i=2}^{N-1} \frac{k_{\text{f}}}{k_{\text{f}} + k_{\text{coll}} + k_{\text{nr},i} + k_{O_2}} \prod_{j=1}^{i-1} \frac{k_{\text{coll}}}{k_{\text{f}} + k_{\text{coll}} + k_{\text{nr},j} + k_{O_2}} \right) \\ &+ \frac{k_{\text{f}}}{k_{\text{f}} + k_{\text{nr},N} + k_{O_2}} \prod_{j=1}^{N-1} \frac{k_{\text{coll}}}{k_{\text{f}} + k_{\text{coll}} + k_{\text{nr},j} + k_{O_2}},\end{aligned} \tag{6}$$

where the summation starts at the initially excited level ($i = 1$) and terminates when the molecule reaches a vibrational state sufficiently close to the thermalized (Nth) level. FQY is equal to the probability of fluorescing from the initial level, plus the probability of colliding downward, times the probability of fluorescing from the ith energy level, plus the probability of fluorescing from the thermalized level (times the probability of colliding downward).

The wavelength dependence enters explicitly through the initial energy calculation; the temperature dependence enters though the collisional frequency and the temperature-dependent non-radiative rate; the pressure dependence enters into the model through the reference collisional frequency and bath gas properties. The baseline model was originally intended to elucidate relative, not absolute fluorescence dependencies; absolute values indirectly depend on k_{isc} and, thus, the absolute measurement of Heicklen [34], which has a significant amount of uncertainty.

3.1.3 Trends

Figures 2, 3, 4 and 5 plot the trends in the baseline fluorescence model which can be summarized as follows:

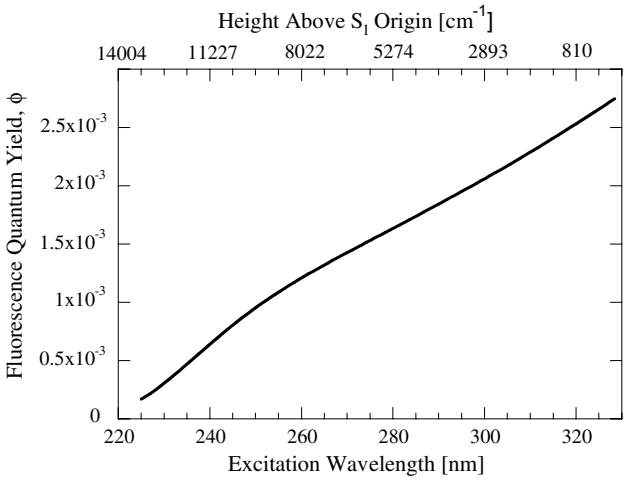

Fig. 2 Excitation energy dependence of absolute FQY as predicted by the model for $P_{\text{ace}} = 2.53$ kPa, at standard temperature and pressure

1. For shorter excitation wavelength (i.e., larger E_{laser}), the "average molecule" is pumped into a higher initial state in S_1 where faster ISC prevails. Therefore, model predictions demonstrate reduced FQY for increasing excitation photon energy as shown in Fig. 2.
2. For increased temperatures, the molecule has more thermal energy in the ground state prior to excitation. For the same excitation wavelength and pressure, the molecule is pumped into a higher initial vibrational state in S_1 where the molecule crosses over to T_1 at a faster rate. Thus, for constant excitation wavelength and pressure, the model predicts an overall decrease in fluorescence with increased temperature as shown in Fig. 3a.
3. For constant excitation wavelength and temperature and increasing pressure, vibrational relaxation dominates over ISC such that the "average molecule" has a higher probability of collisional deactivation in the S_1 manifold. Thus, the "average molecule" in S_1 has a higher probability of fluorescing from these lower vibrational energy levels, since the ISC rate decreases with decreased excited state energy. For constant temperature, model predictions indicate an increase in ϕ with increased pressure shown in Fig. 3b. Further, as shown in Fig. 4, the model predicts a low pressure limit on fluorescence, solely dependent on the initially excited state energy level, which is determined by the combination of temperature and excitation wavelength. It also predicts a high pressure limit on fluorescence, independent of the initial excited state energy level, which reaches a single value asymptote representing complete vibrational relaxation. On an absolute basis, this asymptote is independent of initial height

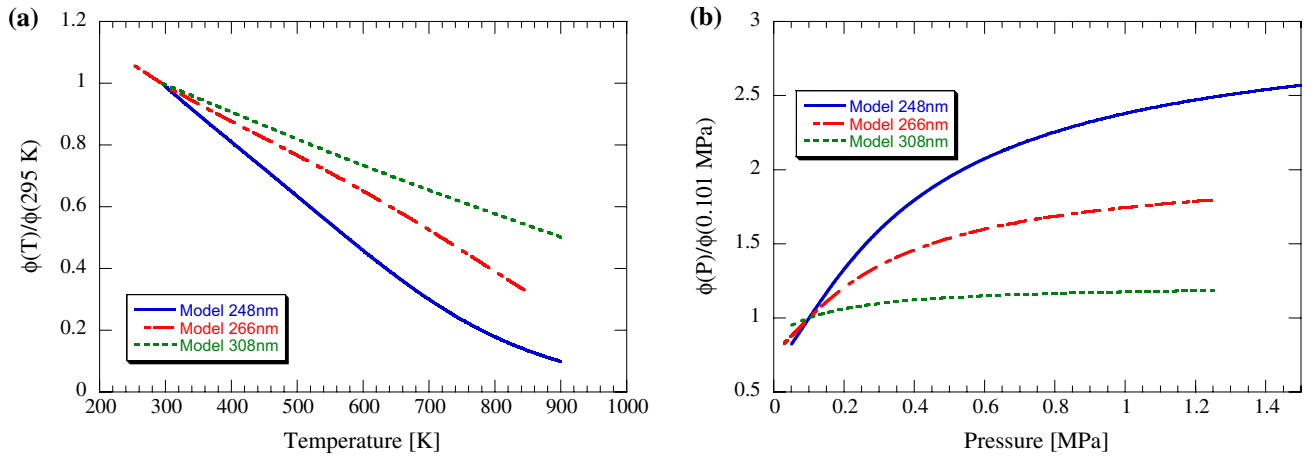

Fig. 3 Relative **a** room pressure, variable temperature dependence and **b** room temperature, variable pressure dependence of acetone FQY in an N_2 gas bas, with varying excitation wavelengths. All points are normalized to 295 K, 0.101 MPa

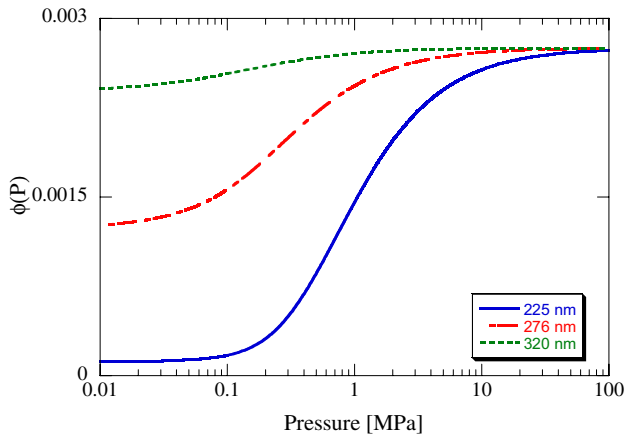

Fig. 4 Model predicted low and high pressure limits on absolute acetone FQY for three excitation wavelengths. For all curves, $T = 295$ K with N_2 as the bath gas

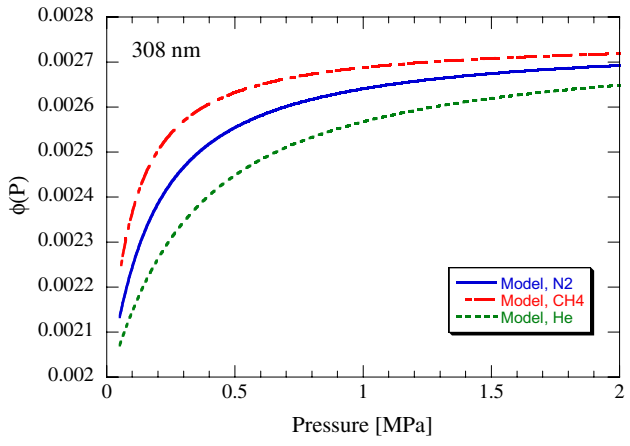

Fig. 5 Model generated absolute bath gas dependencies of acetone fluorescence at 308 nm excitation in N_2, methane (CH_4), and He bath gases. $P_{ace} = 2.53$ kPa, $T = 295$ K for all curves

(as determined by the combination of excitation wavelength and temperature) in S_1. On a relative scale, lower excitation wavelengths will produce more sensitivity to large pressures since fluorescence is weaker at room temperature and pressure.

4. For constant excitation wavelength, temperature, and pressure, for differing bath gases, the model predicts an increase in overall FQY proportional to the number of atoms in the collider. Per Table 1, both the frequency of collision (Z_{coll} or k_{coll}) and the size of the collider influence the overall energy transferred per collision. The product of $Z_{coll}\alpha$ essentially tracks the collisional dependence. For example, nitrogen (N_2) may have a slower collisional frequency than helium (He) gas, but is a bigger molecule and, therefore, yields higher FQY as illustrated in Fig. 5. Meanwhile, the FQY decreases with increasing oxygen content (oxygen number density).

3.2 Predictions for elevated pressure and temperature

In general, it was demonstrated that there is a higher probability of absolute fluorescence from lower vibration levels in S_1 and a lower probability of fluorescence from high vibrational levels. In the limit of high temperature or low excitation wavelength, k_{nr} dominates. As the distribution of excited state molecules reaches higher vibrational levels in S_1, either by increased pumping energy or higher temperature, absolute FQY will on average be higher for a single high pressure. The collisional rate dominates over the non-radiative rate in the limit of high pressure, returning molecules back down to lower vibrational levels where they more easily fluoresce. Data and model both demonstrate this trend. But when initial temperature is simultaneously increased with pressure, competition

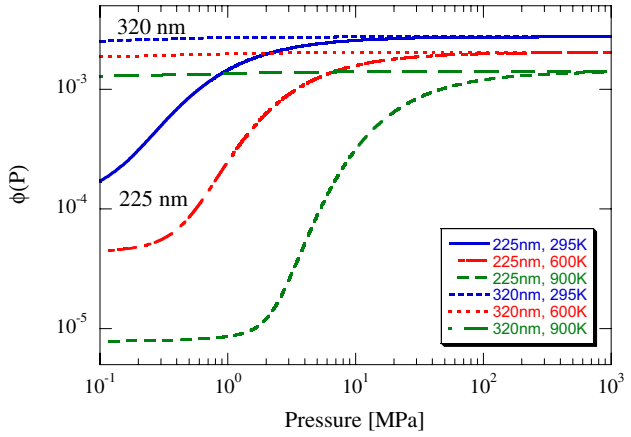

Fig. 6 Model predicted effect of elevated temperature on pressure dependence of acetone fluorescence with varying excitation wavelengths. For all curves, $P_{ace} = 2.53$ kPa with N_2 as the bath gas

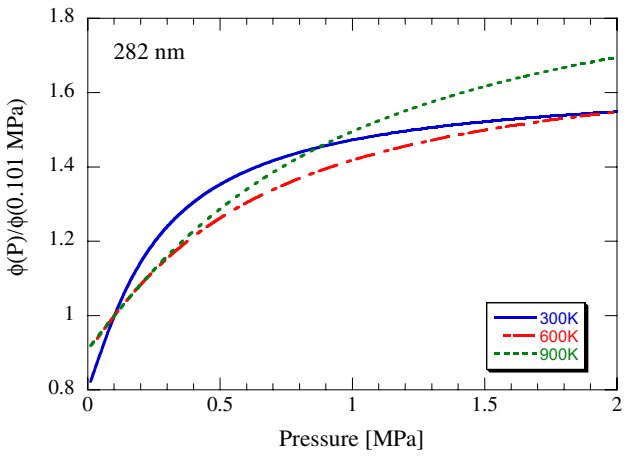

Fig. 7 Effect of elevated temperature on pressure dependence of acetone fluorescence in an N_2 bath gas at 282 nm excitation. For all curves, $T = 295$ K, $P_{ace} = 2.53$ kPa

between k_{nr} and k_{coll} is reintroduced into the photophysics of the system.

Figure 6 plots the effect of elevated temperature on the pressure dependence for acetone at the two edges of the acetone absorption spectrum. As expected, the low pressure asymptote is fixed for a given excitation wavelength and temperature. Interestingly, the model predicts that the high pressure asymptote will be fixed for a given temperature, independent of excitation wavelength. This is due to the fact that $\Delta E_{thermal}$, a quantity that both collisional and non-radiative rates are dependent upon is fixed for a given temperature in the fluorescence calculation. This implies no matter how high the pressure, acetone cannot overcome the non-radiative effect associated with high temperature. Clearly, the model predicts an insensitivity of high temperature on the pressure-dependent fluorescent behavior at long excitation wavelengths and that the collisional effects will dominate over non-radiative effects at shorter excitation wavelengths.

At 282 nm excitation wavelength in the current experimental work [7], it is important to note that, although it is predicted that fluorescence will increase slightly with increasing temperature and pressure, the effect may be much less dramatic than that at previously reported excitation wavelengths. This is due to the fact that 282 nm lies very near to the acetone absorption peak. In Fig. 7, the model predicts a minimal variation in the high pressure asymptotic value at 282 nm excitation.

4 Improved acetone fluorescence modeling

The baseline model fails when pressure and temperature are simultaneously increased, as is evident in the data presented in this work [7], as well as the limited literature data sets. For example, Fig. 8a, b plot model results against the elevated pressure and temperature data from [4] and [7], respectively. For acetone seeded in both air and oxygen at 248 nm excitation, as temperature is increased with increasing pressure, relative fluorescence decreases in the data and as predicted by modeling; the same over-prediction with increasing pressure still prevails [4]. Meanwhile for the 282 nm excitation data from [7], for N_2, the model predicts a weak, but steady increase in fluorescence with increasing temperature, while data show strong evidence for the existence of an isotherm at which fluorescence is maximum. For air, the model predicts an initial quenching behavior where FQY briefly peaks in the intermediate pressure range, followed by a steady increase in fluorescence with increasing temperature. Data indicate that fluorescence gradually increases with pressure and temperature, following the same general behavior as in the case for N_2. Although not shown, data at 282 nm excitation, 700 K exhibit a limit to the positive effect of collisional deactivation on fluorescence where the 700 K pressure trend lies below the room temperature pressure trend, and suggest a maximum isotherm where non-radiative rates begin to dominate again.

In general, the baseline model greatly over-predicts high pressure effects, especially at higher excitation energies. The baseline model especially breaks down in the high pressure range in the presence of oxygen, and data suggest that the oxygen-assisted ISC rate is coupled with the collisional rate for bath gases that contain oxygen. It is also unclear as to whether fluorescence peaks at a given isotherm at constant pressure and then decreases in the presence of oxygen, or follows similar behavior as that of an inert bath gas.

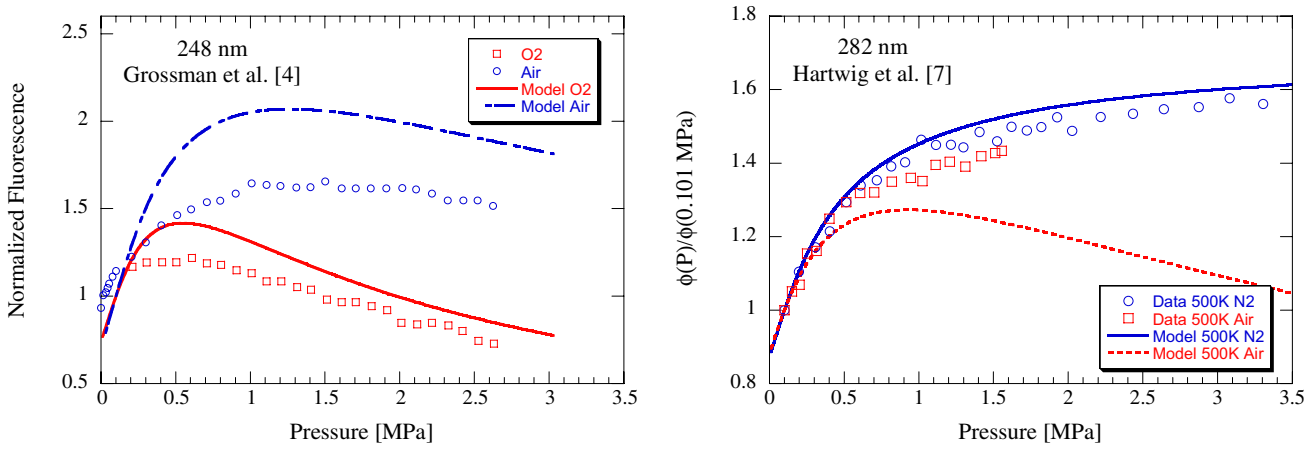

Fig. 8 Relative fluorescence predictions at higher pressures for **a** acetone seeded in air and oxygen at 248 nm excitation, 383 K, $P_{ace} = 1.47$ kPa from Grossman et al. [4] and **b** acetone seeded in N_2 and air at 282 nm excitation, 500 K, $P_{ace} = 4.4$ kPa

The majority of the inabilities of the baseline model to predict fluorescence behavior at higher pressure, temperature, and excitation energies are contained within the initial assumptions in formulating the code. First, model parameters were originally fit to the lower pressure range of [40] and the atmospheric pressure, high temperature data of [1]. Second, since certain non-radiative rates were neglected and the model neglected upward collisions where non-radiative rates are faster, the baseline model will naturally over-predict the FQY. Third, the collisional energy transfer of proportionality, α, was assumed to be the same for N_2, air, and oxygen bath gases. This renders it impossible for the code to recover the collisional effects in mixtures containing differing percentages of oxygen.

4.1 Updated model parameters

As such, comparison between baseline model and new elevated pressure and temperature data warranted model improvements. Rather than simply adjust the model to the current work, model parameters were readjusted globally to include the 4 literature studies at elevated pressure and temperature [3–6]. Results of the global optimization scheme are summarized in Table 2 in the order by which parameters were adjusted. Baseline and newly adjusted rates are presented, along with the average overall error based on minimizing the least squared distance between data and model predictions. Several immediate model improvements are made possible through studies in tracer LIF that were done previously and concurrently with this work, along with a new optimization scheme. For simplicity and ease of computation, re-optimization of model parameters was split into cases with and without oxygen present in the colliding partner. The optimized values of k_f, k_{nr}, $\alpha_{N2,1}$, and $\alpha_{N2,2}$ were simultaneously adjusted and then used to optimize k_{o_2}, $\alpha_{Air,1}$, and $\alpha_{Air,2}$. All other collision constants were adjusted independently with these new rates. Naturally, the most rigorous code would

Table 2 Updated acetone fluorescence model parameters

Model parameter	Baseline value	Error before adjustment (%)	Optimized value	Error after adjustment (%)
k_f [1/s]	8×10^5	6.30	3×10^5	3.08
k_{nr} [1/s]	$-3.82 \times 10^9 + 8.82 \times 10^5$*exp($E$/1650) + 4.08×10^9*exp(E/7.73e4)		$-3.63 \times 10^9 + 4.25 \times 10^5$*exp($E$/1532) + 3.88×10^9*exp(E/88066)	
$\alpha_{N2,1}$, $\alpha_{N2,2}$	0.021, 0		0.021, −0.74	
α_{CH4}	0.03	5.50	0.026	3.64
α_{He}	0.0098	6.70	0.0056	3.42
k_{o_2} [1/s]	3.99×10^{-4} *$k_{coll,O2}$	13.5	6.60×10^{-7}* exp(E/1999)* k_{coll,o_2}	3.74
$\alpha_{Air,1}$, $\alpha_{Air,2}$	0.021, 0		0.045, 0.382	
α_{co_2}	0.021	11.1	0.03	3.02

involve simultaneous re-adjustment of all model parameters. The rationale of using $\alpha_{N2,1}$, $\alpha_{N2,2}$, $\alpha_{\mathrm{Air},1}$, and $\alpha_{\mathrm{Air},2}$ will be introduced in due course.

First, the overall radiative and non-radiative rates and bath gas constant for N_2 were simultaneously re-adjusted. Due to the large amount of available data in the literature at different temperatures, pressures, and excitation wavelengths relative to other bath gases, nitrogen was chosen to update the value for k_{nr}. But as shown in Table 2, the overall least squares difference between baseline and optimized model predictions for the combined effect of these parameters reduced in half from 6.30 to 3.08%.

First, through the work of Koch et al. [42], who conducted the first absolute acetone FQY measurement since the studies of Heicklen [34] and Halpern and Ware [32], a new lower value for the constant rate of fluorescence, k_{f}, is assigned. Second, a modified non-radiative rate is proposed as was done in the work of [5], where the rate was fit to the acetone LIF data at 248 nm excitation, 1–2 MPa and 295–690 K. The bi-exponential behavior of k_{nr} was preserved while only the portion that represents excitation energies higher than 8000 cm^{-1} was modified. However, this rate was only modified in [5] to fit the range of data in that work and it failed to recover the low pressure and temperature data from previous studies. Also, because the k_{nr} value was adjusted to fit data exclusively done in that work, rather than by global optimization, it is unclear as to whether or not the adjusted model parameters can truly track changes in experimental data at high pressure and temperature. Therefore, a new globalized non-radiative rate is proposed in this work to optimize the value over the entire range of all experimental acetone data in N_2. Both the low and high vibrational energy-dependent exponential components of k_{nr} were adjusted, as shown in Fig. 9.

Third, the value for the collisional constant of proportionality for N_2 was adjusted to include a modified temperature dependence. In conditions at high temperature and shorter excitation wavelengths where the baseline model diverged from experimental data the most, using the absolute fluorescence data from [3] as a guide, it was desired to modify the collision constant for N_2. It is hypothesized that N_2 may have a decreased collisional efficiency at higher temperatures than what was previously anticipated from the model of [46]. Although there is no a priori knowledge of a temperature-dependent collisional transfer for acetone, results here are extended from the work done on ethyl acetate where ΔE_{Coll} was shown to decrease with increasing temperature and follow a general functional form of:

$$\langle \Delta E_{\mathrm{Coll}} \rangle \propto T^{-n} \tag{7}$$

where the exponent n is chosen to fit high temperature data of [46]. In that work, for ethyl acetate dilute in N_2 over the range of 340–850 K, the exponent was chosen as $n = 0.4$. For this work, the assumed collisional constant of proportionality for N_2 in the baseline model is adjusted to take on the following functional form:

$$\alpha_{N2} = \alpha_{N2,1}\left(\frac{T}{300}\right)^{\alpha_{N2,2}} \tag{8}$$

Examination of the elevated temperature and pressure absolute fluorescence data from [3] revealed that acetone diluted in N_2 exhibits a relatively strong negative temperature dependence on collision efficiency. As such, the exponent in Eq. 8 fits accordingly:

$$\begin{aligned} \alpha_{N2,1} &= 0.021 \\ \alpha_{N2,2} &= -0.74 \end{aligned} \tag{9}$$

and plotted in Fig. 10a, along with the baseline model value.

Fourth, all other collisional constants of proportionality without oxygen were modified using the newly obtained fluorescence and non-radiative rates. Only room temperature data for He and CH_4 existed in the literature; therefore, no temperature dependence on these collisional constants is justified at this time. Still, these values were optimized based on available data and updated as shown in Table 2.

Then, bath gases containing O_2 were addressed. Upon gathering all available data for acetone in bath gases containing O_2, it was revealed that the largest pool of data existed for an air bath gas. Therefore, as in the case of the non-radiative rate, the value for $k_{\mathrm{o_2}}$ and the collisional constant for air were adjusted simultaneously. α_{Air} is plotted in Fig. 10b.

A new O_2 quenching rate is proposed, which was based on the studies of [36]. The newly adjusted rate takes into account collisions due to bath gases containing oxygen as

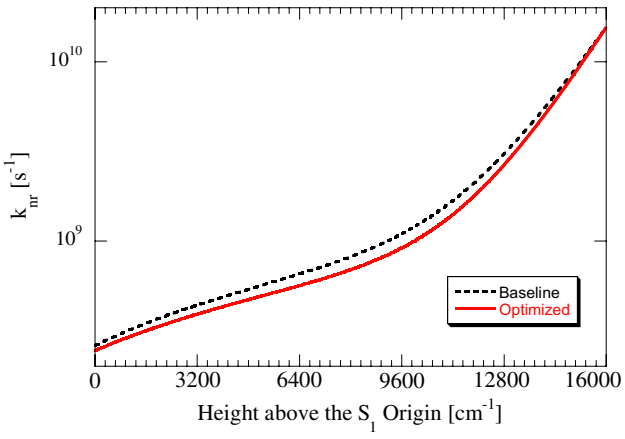

Fig. 9 Comparison between the baseline and optimized non-radiative rate as a function of excess energy above the excited singlet origin

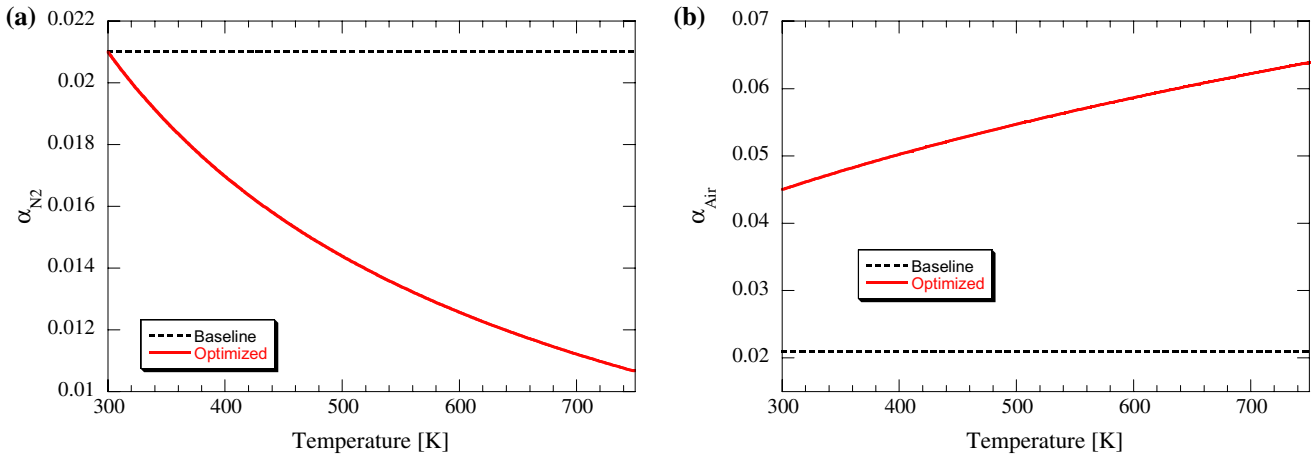

Fig. 10 Optimized collisional constants of proportionalities for **a** N_2 and **b** air as a function of temperature

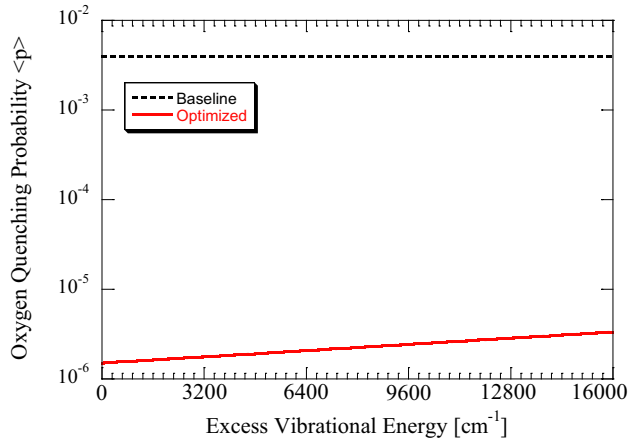

Fig. 11 Optimized model generated oxygen quenching probability

well as the oxygen-assisted ISC component in accordance with the high excitation energy and temperature data of [5] and the current work. In [5], different quenching rates were proposed for air and carbon dioxide (CO_2). The new global quenching rate proposed here takes into account pressure, temperature, excitation wavelength, and oxygen number density over the available air bath gas data in the following exponentially decaying form:

$$k_{o_2} = \left[k_1 \exp(E/k_2)\right] k_{\text{coll},o_2} \tag{10}$$

where k_{coll,O_2} is listed in Table 1. A single exponential function for the oxygen quenching probability was chosen to account for the energy-dependent assisted ISC rate. Interestingly, as shown in Fig. 11, the newly optimized rate resembles a constant for oxygen quenching acetone fluorescence, owing to its weak energy dependence.

To recover the temperature dependence of the collision efficiency for air, a functional form similar to that of N_2 is chosen:

$$\alpha_{\text{Air}} = \alpha_{\text{Air},1}\left(\frac{T}{300}\right)^{\alpha_{\text{Air},2}}. \tag{11}$$

Consistent with data in this work, as shown in Fig. 10b, air is shown to have a weak positive temperature collision efficiency; this behavior is much more common of bath gas molecules [45, 47]. A new value for acetone in air is proposed, along with a positive exponent, as shown in Table 2. On average, the optimized model predicts that air will transfer twice as much energy per collision as N_2 at room temperature.

Finally in the optimization scheme, all other bath gases containing oxygen were addressed. Since elevated temperature data for CO_2 existed in the literature, a new optimized collisional constant was fit to the data as shown in Table 2; it was found that a single constant fitting term provided adequate fit to the CO_2 data. Since no new experiments for acetone in a pure O_2 bath gas were conducted, the collisional constant was not adjusted for temperature dependence. As shown, overall error between model predictions and experimental data was reduced below 4% in the presence of oxygen colliders.

In addition to the global optimization of model parameters, two other general model improvements were included in accordance with the suggestions of [5]. Collisions between polar and nonpolar molecules were calculated, and real bath gas functions were used to replace the ideal gas behavior assumed in previous work [15, 48, 49]. Unfortunately, these two adjustments produced little to no effect on fluorescence results and were thus omitted from subsequent calculations. Regarding recent attempts at model

improvements for other ketones such as 3-pentanone and biacetyl, the k_{nr} rate proposed by [45] was unmodified in the work of [50]; only the bath gas collisional transfer coefficient and probability of quenching were modified to fit the model curves.

4.2 Comparison with data

After optimization of the model parameters, discrepancies in this and previous work between model predictions and experimental results for the coupled elevated temperature and pressure effects on acetone fluorescence may now be readdressed. First, acetone LIF data in bath gases not conducted in this work are presented. Figure 12a shows the optimized results for data taken at 248 nm excitation in He and CH_4 bath gases [51]. Clearly, the model and data match well. Figure 12b presents new model results against elevated pressure and temperature CO_2 data from [5]. As shown, there is very good agreement when using the newly optimized rates.

Secondly, the room temperature, variable pressure range and room pressure, variable temperature range for acetone in N_2 was re-examined. As shown in Fig. 13a, b, the optimized model clearly tracks the fluorescence data well throughout the entire range of temperatures, pressures, and excitation wavelengths. Maximum deviation occurs at longer excitation wavelengths.

Third, the optimized model was applied to the current elevated temperature and pressure range examined in this work. Results are plotted in Figs. 14a, b. As shown, the new model parameters successfully account for the maximum fluorescing isotherm in N_2. Both data and model show that the relative fluorescence pressure trace at 400 K rises above the room temperature pressure trace, and then slowly decreases with increasing temperature for 282 nm excitation. In an air bath gas, there is also good agreement between data and

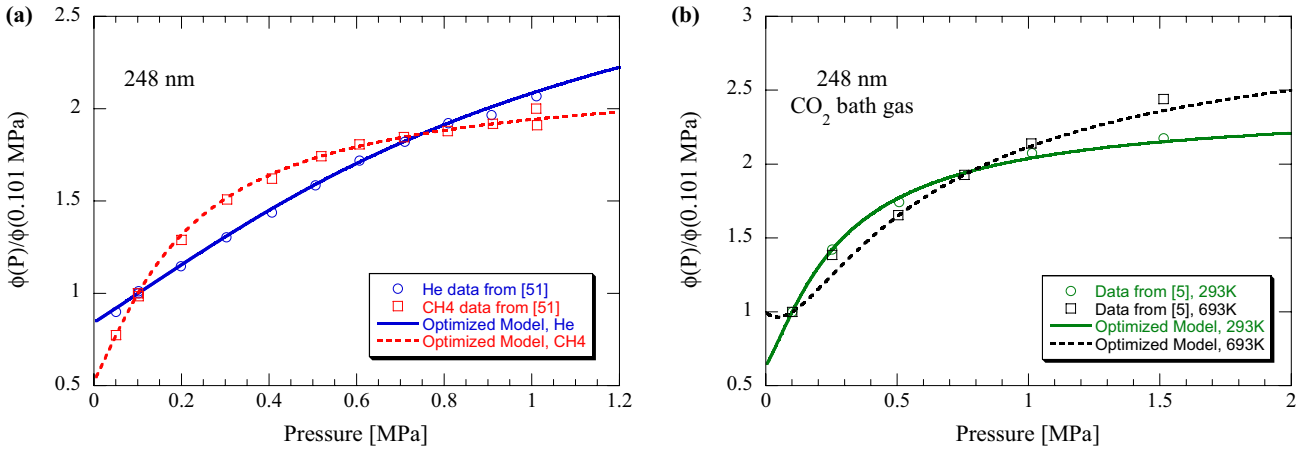

Fig. 12 Optimized model results for **a** He and CH_4 bath gases against data from [51] and **b** CO_2 bath gas against data from [5]

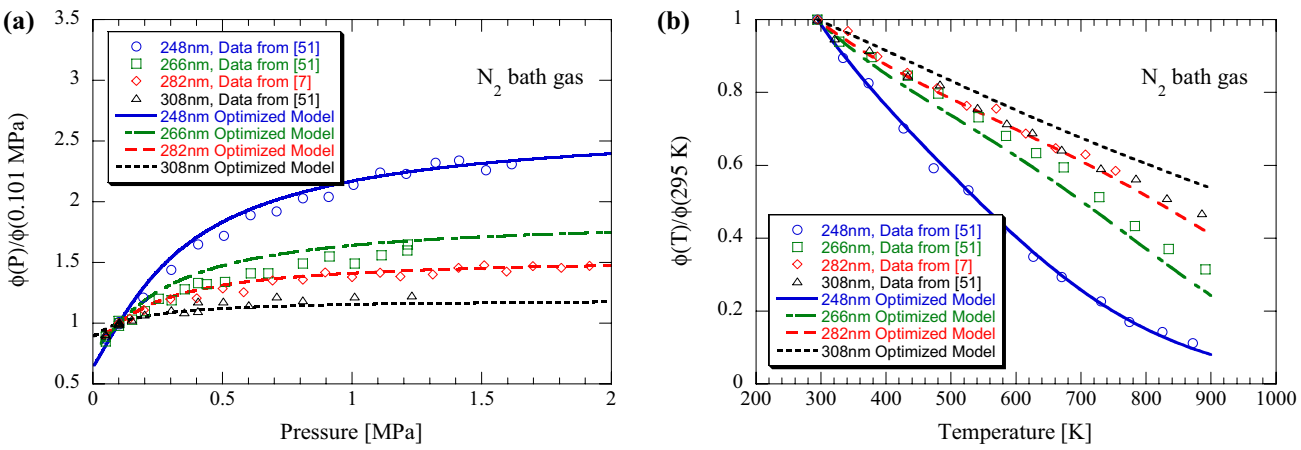

Fig. 13 Optimized model results for acetone fluorescence in an N_2 bath gas for **a** room temperature, elevated pressure, and **b** room pressure, elevated temperature

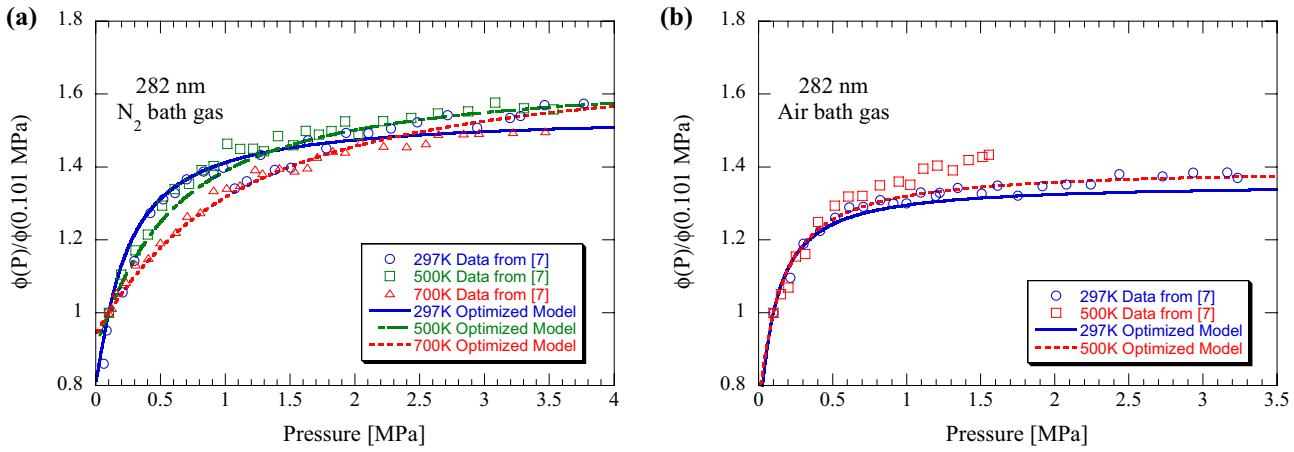

Fig. 14 Optimized model results for acetone fluorescence in elevated pressure and temperature using **a** N_2 and **b** air as bath gases

model. It shows that air has a positive collision efficiency at elevated temperatures, and although the model does successfully track this dependence, it does slightly under-predict the magnitude of this effect. More elevated temperature data in an air bath gas are needed to fully examine this trend. Although not shown here for brevity, the new optimized model matches well with data from [6].

Finally, for illustrative purposes, and to interpret anticipated signal levels in high temperature and pressure environments, especially where both may vary simultaneously, one can interpolate both experimental and model results to map out fluorescence as a function of temperature and pressure. Interpolated model results, which are based on the experimental data in [7], are plotted in Fig. 15. As shown for 282 nm excitation, when acetone LIF is used in elevated pressure combustion systems, the high pressure can counter the signal degradation due to elevated temperature. For example, the normalized FQY value of 1 persists at elevated temperatures up to ~600 K at pressures beyond 25 atm.

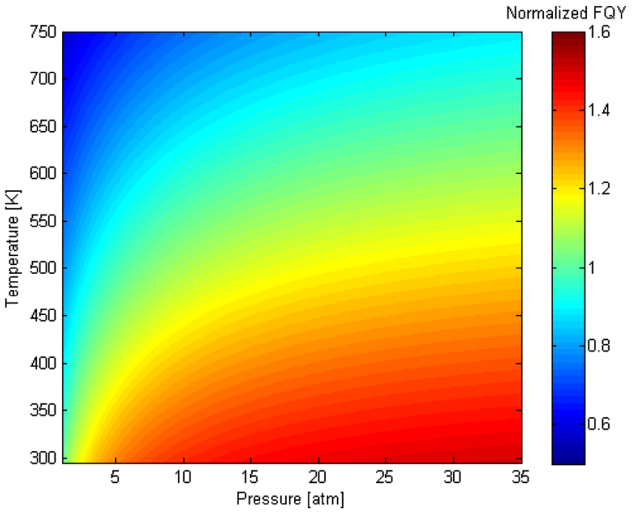

Fig. 15 Interpolated two dimensional model results for acetone fluorescence in an N_2 bath gas for 282 nm excitation. The color bar indicates lines of constant normalized fluorescence quantum yield. All fluorescence points are normalized by the value obtained at 295 K, 0.101 MPa

5 Conclusions

Elevated temperature and pressure experimental data in [7] and the four available literature studies [3–6] contradict the baseline model assumption that fluorescence continually increases at elevated pressures and temperatures. Instead, collisional effects are in fact saturated at high enough temperatures such that k_{nr} causes sufficient crossover to the triplet, even at high pressure. As a result, the three parameters, k_{nr}, α, and $\langle p \rangle$, of the baseline model have been optimized, along with an updated k_f based on global consideration to account for vibrational energy levels in excess of 7000 cm^{-1} in N_2 and air bath gases. The collisional constants of proportionality which govern vibrational relaxation are shown to be temperature-dependent at elevated pressures. An improved oxygen-enhanced intersystem crossing model improves disparity between model and oxygen-content bath gases.

Results show an improved agreement between predicted model values and both low temperature and pressure experimental data from previous work, as well as elevated temperature and pressure data from this work and other studies. Also, the general over-prediction of the pressure dependence on acetone fluorescence was significantly improved through model global optimization. As more data become available, especially at elevated temperatures and pressures, the values of the parameters should be re-examined concurrently.

Aside from adding to the tracer LIF consolidated database by obtaining more data at elevated pressure and temperature, and different excitation wavelengths and bath gases, future work should include additional improvement on fluorescence modeling. For example, further investigation is required on the temperature functionality of the collision transfer constant of proportionality, α, for each bath gas. Secondly, once data have been obtained for many bath gases with and without the presence of oxygen, the k_{nr} rate could be modified to account for both low and high vibrational energy channels. Third, there is no fluorescence model for biacetyl. Due to the recent renewed interest in this tracer as a diagnostic in internal combustion engines, it would beneficial to formulate its own fluorescence model. Once acetone, 3-pentanone, and biacetyl fluorescence have been characterized over a wide range of experimental conditions, global considerations regarding general ketone fluorescence modeling may be completed. Ultimately, the goal of these improvements is in being able to extract the non-radiative rate, oxygen quenching rate, and the collisional constants of proportionality of each bath gas as physical observables. Nevertheless, even in its current state the newly optimized acetone photophysical mechanism can be confidently extended to model acetone fluorescence in elevated pressure and temperature systems where acetone LIF is used as a diagnostic technique to extract physical variables of interest.

References

1. M.C. Thurber, *Acetone laser-induced fluorescence for temperature and multiparameter imaging in gaseous flows*. PhD thesis, Stanford University Mechanical Engineering Department, 1999
2. A.C. Eckbreth, *Laser diagnostics for combustion temperature and species*, 2nd edn. (Gordon & Breach Publishers, Philadelphia, 1996)
3. F. Ossler, M. Alden, Appl. Phys. B **64**, 493–502 (1997)
4. F. Grossman, P.B. Monkhouse, M. Ridder, V. Sick, J. Wolfrum, Appl. Phys. B **62**, 249–253 (1996)
5. A. Braeuer, F. Beyrau, A. Leipertz, Appl. Opt. **45**, 4982–4989 (2006)
6. M. Loffler, F. Beyrau, A. Leipertz, Appl. Opt. **49**, 37–49 (2010)
7. J.W. Hartwig, G. Mittal, K. Kumar, and C.J. Sung, Appl. Phys. B. **123**, (2017). doi:10.1007/s00340-017-6774-z
8. E.K.C. Lee, R.S. Lewis, Adv. Photochem. **12**, 1–95 (1980)
9. W.R. Ware, S.K. Lee, J. Chem. Phys. **49**, 217–220 (1968)
10. D.A. Hansen, E.K.C. Lee, J. Chem. Phys. **62**, 183–189 (1975)
11. C. Schulz, V. Sick, Prog. Energy Combust. Sci. **31**, 75–121 (2005)
12. M. Baba, I. Hanazaki, Chem. Phys. Lett. **103**, 93–97 (1983)
13. H. Zuckermann, Y. Haas, Chem. Phys. **163**, 193–208 (1992)
14. D.W. Liao, A.M. Mebel, M. Hayashi, Y.J. Shiu, Y.T. Chen, S.H. Lin, J. Chem. Phys. **111**, 205–215 (1999)
15. R.B. Bird, W.E. Stewart, E.N. Lightfoot, *Transport phenomena*, 2nd edn. (Wiley, Hoboken, 2007)
16. D.J. Wilson, B. Noble, B. Lee, J. Chem. Phys. **34**, 1392–1396 (1960)
17. M.J.G. Borge, J.M. Figuera, J. Luque, Study of the emission of the excited acetone vapour at intermediate pressures. Spectrochim. Acta **46A**, 617–621 (1990)
18. G.B. Porter, B.T. Connelly, Kinetics of excited molecules. II. Dissociation processes. J. Chem. Phys. **33**, 81–85 (1960)
19. J. Troe, J. Chem. Phys. **77**, 3485–3492 (1982)
20. H. Hippler, J. Troe, H.J. Wendelken, J. Chem. Phys. **78**, 6709–6717 (1983)
21. H. Hippler, J. Troe, H.J. Wendelken, J. Chem. Phys. **78**, 6718–6723 (1983)
22. I. Oref, D.C. Tardy, Chem. Rev. **90**, 1407–1445 (1980)
23. H. Hippler, B. Otto, J. Troe, Berichte der Bunsen-Gesellschaft für Physikalische Chemie **93**, 428–434 (1989)
24. G.H. Kohlmaier, B.S. Rabinovitch, J. Chem. Phys. **38**, 1692–1708 (1963)
25. M.J. Rossi, J.R. Pladziewicz, J.R. Barker, J. Chem. Phys. **78**, 6695–6708 (1983)
26. J. Troe, J. Phys. Chem. **87**, 1800–1804 (1983)
27. G.M. Breuer, E.K.C. Lee, J. Phys. Chem. **75**, 989–990 (1971)
28. R.G. Shortridge, C.F. Rusbult, E.K.C. Lee, J. Am. Chem. Soc. **93**, 1863–1867 (1971)
29. J.C. Hsieh, C.S. Huang, E.C. Lim, J. Chem. Phys. **60**, 4345–4353 (1974)
30. Y. Hirata, E.C. Lim, J. Chem. Phys. **69**, 3292–3296 (1978)
31. H.J. Groh, G.W. Luckey, W.A. Noyes, J. Chem. Phys. **21**, 115–118 (1953)
32. A.M. Halpern, W.R. Ware, J. Chem. Phys. **34**, 1271–1276 (1971)
33. R.A. Copeland, D.R. Crosley, Chem. Phys. Lett. **115**, 362–368 (1985)
34. J. Heicklen, Am. Chem. Soc. **81**, 3863–3866 (1958)
35. F. Ossler, M. Alden, Appl. Phys. B **64**, 493–502 (1997)
36. W.M. Nau, J.C. Scaiano, J. Phys. Chem. **100**, 11360–11367 (1996)
37. C. Grewer, C. Wirp, M. Neumann, H.D. Brauer, Berichte der Bunsen-Gesellschaft für Physikalische Chemie **98**, 997–1003 (1994)
38. R.G. Brown, D. Phillips, J. Chem. Soc. Faraday Trans. **2**(70), 630–636 (1973)
39. J. Heicklen, W.A. Noyes, J. Am. Chem. Soc. **81**, 3858–3863 (1958)
40. L.S. Yuen, J.E. Peters, R.P. Lucht, Optics **36**, 3271–3277 (1997)
41. M.C. Thurber, F. Grisch, B.J. Kirby, M. Votsmeier, R.K. Hanson, Appl. Opt. **37**, 4963–4978 (1998)
42. J.D. Koch, R.K. Hanson, W. Koban, C. Schulz, Appl. Opt. **43**, 5901–5910 (2004)
43. J.C. Hsieh, E.C. Lim, J. Chem. Phys. **61**, 736–737 (1974)
44. G.W. Robinson, R.P. Frosch, J. Chem. Phys. **38**, 1187–1203 (1962)
45. J.D. Koch, *Fuel tracer photophysics for quantitative planar laser-induced fluorescence*. PhD thesis, Stanford University, 2005
46. T.C. Brown, J.A. Taylor, K.D. King, R.G. Gilbert, J. Phys. Chem. **87**, 5214–5219 (1983)
47. J.H. Kiefer, S. Santhanam, N.K. Srinivasan, R.S. Tranter, S.J. Klippenstein, M.A. Oehlschlaeger, Proc. Combust. Inst. **30**, 1129–1135 (2005)
48. L. Monchick, E.A. Mason, J. Chem. Phys. **35**, 1676–1697 (1961)
49. R.S. Brokaw, I&EC Process Des. Dev. **8**, 240–253 (1969)
50. V. Modica, C. Morin, P. Guibert, Appl. Phys. B **87**, 193–204 (2007)
51. M.C. Thurber, R.K. Hanson, Appl. Phys. B **69**, 229–240 (1999)